Journal of Experimental Botany, Vol. 77, No. 4 pp. 1279–1292, 2026
https://doi.org/10.1093/jxb/eraf470 Advance Access Publication 24 October 2025

RESEARCH PAPER

Turgor loss in vessel-associated parenchyma cells increases xylem vulnerability to embolism

Martina Tomasella[1,*], Steven Jansen[2], Chiara Giacomin[1], Enrico Boccato[1], and Andrea Nardini[1]

[1] Department of Life Sciences, University of Trieste, Trieste 34127, Italy
[2] Institute of Botany, Ulm University, Ulm 89081, Germany

* Correspondence: martina.tomasella@units.it

Received 7 February 2025; Accepted 20 October 2025

Editor: Kathy Steppe, Ghent University, Belgium

Abstract

Drought-induced depletion of non-structural carbohydrates has been reported to affect xylem hydraulic vulnerability, which in turn is frequently correlated with water potential at turgor-loss point. Given that non-structural carbohydrate depletion can impair osmoregulation, we hypothesised that vessel-associated parenchyma cells (VACs) that undergo drought-induced turgor loss and plasmolysis could facilitate gas movement and the formation of xylem embolism. Plasmolysis was induced in wood parenchyma of *Populus nigra* stems of mature trees and potted plants by radial injection or axial perfusion with a polyethylene glycol solution at low osmotic potential. The effect of polyethylene glycol on embolism resistance was assessed using the gas injection technique followed by classic hydraulic quantification of embolism, as well as with flow-centrifuge measurements. Light and transmission electron microscopy confirmed the occurrence of plasmolysis of VACs in osmotically treated samples, while hydraulic measurements revealed an increase in xylem vulnerability to embolism upon induction of plasmolysis, raising the loss of hydraulic conductivity by ~20–40%. The results therefore support the hypothesis that the maintenance of cell turgor in VACs is critical for xylem hydraulic integrity under drought. We speculate that plasmolysis of VACs could promote gas movement to functional vessels via vessel–parenchyma pits, increasing the likelihood of embolism propagation.

Keywords: Black poplar, drought, embolism resistance, osmotic potential, pit membrane, plasmolysis, *Populus nigra*, turgor loss, vessel-associated parenchyma cell (VAC), vessel–parenchyma pit.

Introduction

The xylem comprises a network of conduits consisting of dead cells that ensure long-distance water transport under negative pressure from the roots to the leaves. The disruption of xylem water transport by embolism formation can occur under intense/prolonged drought, and can lead to desiccation of the crown or even to plant death (Anderegg *et al.*, 2012; Nardini *et al.*, 2013; Adams *et al.*, 2017). Xylem embolism is caused by propagation of gas from a gas-filled apoplastic compartment to a functional water-filled conduit, and occurs when a critical pressure difference between these compartments is exceeded

Abbreviations: π, osmotic potential; Ψ_{tlp}, water potential at turgor loss point; P_{50}, water potential at 50% loss of xylem hydraulic conductance; PEG, polyethylene glycol; PLC, percentage loss of xylem hydraulic conductivity; T_{pm}, pit membrane thickness; VAC, vessel-associated parenchyma cell.

(Zimmermann, 1983; Cochard *et al.*, 1992; Salleo *et al.*, 1992). This pressure threshold has been suggested to depend on the pit-membrane thickness and the amount of intervessel pit membrane area within a given vessel (Kaack *et al.*, 2019, 2021). Gas diffusion processes are also suggested to be connected with embolism spread (Guan *et al.*, 2021; Silva *et al.*, 2024), but mechanistic details of how exactly gas movement leads to embolism remain largely unclear.

Independent of the actual biophysics behind the process, xylem embolism formation requires the presence of a pre-existing gas phase that propagates into a nearby functional xylem conduit. In this respect, *in vivo* X-ray micro-computed tomography (CT) analyses have frequently shown that as drought progresses, embolism spreads radially from the older wood close to the pith towards the cambium (e.g. Brodersen *et al.*, 2013; Choat *et al.*, 2016; Secchi *et al.*, 2021). This pattern might depend on poorly lignified protoxylem conduits (i.e. those in proximity to the pith), which would easily embolize due to partial lack of secondary walls and to ruptures that occur during extension growth (Choat *et al.*, 2005).

It is well established that embolism resistance is influenced by xylem anatomical features, such as conduit density, arrangement and connectivity (Pittermann *et al.*, 2006; Mrad *et al.*, 2018; Avila *et al.*, 2023), and by interconduit pit characteristics and ultrastructure, such as pit-membrane thickness and pore constriction sizes (Jansen *et al.*, 2009; Lens *et al.*, 2011; Li *et al.*, 2016). In angiosperms, intervessel pit membranes appear to play a major role in the spread of embolism from one conduit to another (Kaack *et al.*, 2019; Zhang *et al.*, 2020).

The water potential that induces 50% loss of xylem hydraulic conductivity (P_{50}) and the water potential at the turgor-loss point (Ψ_{tlp}) have been described as good predictors of tree drought tolerance (Nardini *et al.*, 2013; Powell *et al.*, 2017; Petruzzellis *et al.*, 2022). Indeed, species from xeric habitats tend to display lower P_{50} values compared to those occupying mesic habitats (Maherali *et al.*, 2004; Choat *et al.*, 2012). With some exceptions (e.g. in some grapevine cultivars; Sinclair *et al.*, 2024), Ψ_{tlp} is often associated with species-specific drought adaptation, with lower values typically recorded for species inhabiting water-limited environments (Bartlett *et al.*, 2014; Zhu *et al.*, 2018). Interestingly, P_{50} and Ψ_{tlp} are frequently correlated with each other (e.g. Bartlett *et al.*, 2016; Christoffersen *et al.*, 2016; Chen *et al.*, 2021; De Guzman *et al.*, 2021), although this relationship changes for highly drought-tolerant species with $P_{50}<-5$ MPa (e.g. Martin-StPaul *et al.*, 2017). This correlation has usually been interpreted as evidence of coordination between traits underlying species-specific drought tolerance at the apoplastic (P_{50}) and symplastic (Ψ_{tlp}) levels, without necessarily suggesting the existence of a direct mechanistic linkage.

Besides drought adaptation, plant acclimation strategies to water shortage rely on decreases of both Ψ_{tlp} and P_{50}. Seasonal variations of Ψ_{tlp}, based on active osmoregulation, have often been described as key drivers of plant acclimation to water stress (Nardini *et al.*, 2003; Turner, 2018). Interestingly, seasonal plasticity in stem P_{50} has also been reported in Chaparral shrubs (Jacobsen *et al.*, 2007), in eight grapevine species/cultivars (Charrier *et al.*, 2018), in the conifer *Pinus halepensis* (Feng *et al.*, 2023), as well as in six temperate woody angiosperms (Ma *et al.*, 2024). Seasonal P_{50} shifts have also been observed in grapevine leaves (Sorek *et al.*, 2021). Feng *et al.* (2023) found seasonal coordination between P_{50} and Ψ_{tlp}, whereas shifts in P_{50} of deciduous species from Mediterranean and temperate habitats were found to be more pronounced than those in Ψ_{tlp} (Sorek *et al.*, 2022). Coordination between the two parameters has also been observed in trees subjected to experimental drought induced by rainfall exclusion (Tomasella *et al.*, 2017; Moreno *et al.*, 2024). Based on these findings, the question arises of whether a more direct mechanistic link could exist between Ψ_{tlp} and P_{50}, rather than a temporal co-occurrence of osmoregulation and hydraulic adjustments under drought stress.

As noted above, osmoregulation lowers the turgor-loss point during drought (Blum, 2017). This process includes accumulation of osmotically active compounds such as inorganic ions and some amino acids, but also soluble non-structural carbohydrates (NSCs) (Hartmann and Trumbore, 2016; Tomasella *et al.*, 2020). In addition, NSCs are the primary energy source that drive cellular active transport of osmotic solutes (Dietze *et al.*, 2014). Indeed, NSC-depleted plants show less-negative Ψ_{tlp} even in well-hydrated conditions, and impaired osmoregulation capacity under drought (Sapes *et al.*, 2021). There is also evidence supporting a possible role for stem NSCs in maintaining plant hydraulic integrity under drought (Bloemen *et al.*, 2016; Tomasella *et al.*, 2020). As an example, prolonged shading induces stem NSC depletion and increased xylem hydraulic vulnerability in *Populus nigra* saplings, without any apparent changes in wood anatomy and intervessel pit traits (Tomasella *et al.*, 2021). Embolism formation increases under drought even when only the stems are covered with aluminium foil to exclude light, thus invoking a role for stem photosynthesis (which locally provides additional NSCs) in maintaining plant hydraulic function under drought, for example in *P. nigra* (De Baerdemaeker *et al.*, 2017) and in *Fraxinus ornus* (Natale *et al.*, 2023). Despite these convergent findings, a mechanistic explanation linking hydraulic safety and NSC availability is still missing (Tomasella *et al.*, 2020). We therefore aimed to clarify if impaired osmoregulation in vessel-associated parenchyma cells (VACs) under low-NSC conditions might be involved in this phenomenon.

VACs differ both anatomically and functionally from parenchyma cells more distant from the vessels. They display an amorphous layer, which is a pecto-cellulosic porous film that apparently ensures the connection between the plasma membrane and the cell wall, thus creating an apoplastic continuum (Klepsch *et al.*, 2016). Moreover, they are connected to vessels by half-bordered pits through which they can exchange water, hormones, and several solutes (e.g. sugars,

Table 1. Schematic overview of the performed experiments

Name of the experiment	Objective	Plant material	Methods
Preliminary Test	Verification of plasmolysis occurrence in VACs upon osmotic treatment	Stems of potted plants	Osmotic treatment of radial wood sections with PEG or with mannitol. Light microscope observation of VAC plasmolysis via Neutral Red staining of vacuole
Test 1	Verification of plasmolysis in VACs upon osmotic treatment and observation of ultrastructural patterns	Stems of potted plants	Osmotic treatment of wood samples. TEM observation of plasmolysis in VACs
Test 2	Plasmolysis visualisation and quantification in VACs upon PEG treatment through stem pressurisation	Stems of potted plants	Stem pressurisation with a PEG solution and embolism induction through a pressure collar. TEM observation of plasmolysis in VACs
Experiment 1	Effect of VACs plasmolysis on xylem vulnerability to embolism	Cut branches of mature trees (Trieste) Stems of intact potted plants	Branch/stem pressurisation with a PEG solution and embolism induction through a pressure collar, as developed in Test 2. Quantification of percentage loss of xylem hydraulic conductivity by classic hydraulic conductivity measurements
Experiment 2	Effect of VACs plasmolysis on xylem vulnerability to embolism	Cut branches from of mature trees (Ulm)	Xylem perfusion with a PEG solution. Xylem vulnerability curves using a flow centrifuge

VACs, vessel-associated parenchyma cells; PEG, polyethylene glycol 6000.

ions; Morris *et al.*, 2018b) with the xylem sap. Although VACs are in direct contact with vessels, it remains unknown whether turgor loss in these parenchyma cells affects xylem hydraulic function under drought. Upon turgor loss, protoplasm dehydration causes the retraction of the plasma membrane from the cell wall, thus disrupting the physical and functional continuity between cells. This phenomenon, known as plasmolysis, was thoroughly studied in several cell types in the past century (see Oparka, 1994 for a review) but, to our knowledge, there is a considerable lack of information on the structural changes that ultimately occur specifically in VACs undergoing plasmolysis, and on their possible functional consequences on water transport.

We hypothesise that a fairly large gas-filled volume might be generated in proximity to functional conduits upon VAC plasmolysis. This phenomenon is usually reversible and does not necessarily imply cell death (Oparka, 1994). Based on similarities in structure and composition between vessel–parenchyma and intervessel pit membranes (Morris *et al.*, 2018b), the gas reservoir generated upon plasmolysis might favour gas propagation into the vessel lumen via vessel–parenchyma pits, thus increasing the likelihood of embolism formation, similar to embolism propagation from an embolised xylem conduit to an adjacent functional one (Guan *et al.*, 2021; Silva *et al.*, 2025). In this study, we tested this hypothesis by examining whether plasmolysis in VACs could be a causal factor of increased xylem vulnerability to embolism formation. Plasmolysis was induced in wood parenchyma cells of *P. nigra* branches or stems, either by radial injection or xylem perfusion of a polyethylene glycol solution at low osmotic potential, and the subsequent effects on embolism formation were assessed with two different methods, namely gas injection followed by classic hydraulic quantification of percentage loss of xylem hydraulic conductivity and by flow-centrifuge measurements of xylem vulnerability to embolism. In addition, the occurrence of plasmolysis and its characteristics in VACs were observed with both light microscopy on vitally stained samples and with TEM.

Materials and methods

Plant material

Experiments were performed on *Populus nigra* using the following plant material. Potted plants were used for microscopy observations and for part of Experiment 1, branches from three mature trees growing near to a parking lot at the University of Trieste (Italy; 45.664615 N, 13.797323 E) were used for part of Experiment 1, and branches from a plantation located near the Blau river in Ulm (Germany; 48.402650 N, 9.951067 E) were used for Experiment 2. On 20 March 2024, 50 1-year-old plants derived from stem cuttings (provided by a regional forestry nursery: Vivai Pascul, Regional Forestry Service, Tarcento, Italy) were transplanted into 3.5 l pots filled with a lightweight substrate (TMLight, Harpo Spa., Trieste, Italy), and grown in a greenhouse at the University of Trieste under natural daylight. Plants were irrigated to field capacity through an automatic drip-irrigation system delivering water two times a day (morning and evening). From transplant to final harvest, the mean daily temperature in the proximity of the potted plants was 19.0±3.5 °C and the relative humidity was 65±11%, as monitored on an hourly basis with a EL-USB-2 datalogger (Lascar Electronics Inc., Salisbury, UK).

Microscopy observations of osmotically induced plasmolysis in vessel-associated cells

A set of experiments was planned to develop a method to induce and observe plasmolysis in the VACs (see Table 1). In a Preliminary Test, *in vitro* light microscopy observations of plasmolysis in stem-wood parenchyma of *P. nigra* were conducted at the University of Trieste following the protocol of Enns *et al.* (2000) with some modifications. In brief, short segments of 1-year-old stems were sampled from the potted plants. Thin radial sections were hand-cut with a razor blade under a potassium phosphate buffer solution (PPB; 0.025 M, pH 7.8) and left in the same solution for 45 min. The samples were then immersed for 15 min in a

0.1% m/V neutral red solution (Sigma-Aldrich) in PPB to stain the vacuoles, and then rinsed several times in PPB. The sections were mounted on slides in PPB and observed under a Zeiss Primostar 3 light microscope to find intact VACs, which were distinguishable due to the presence of large, circular vacuoles. Afterwards, the sections were successively immersed in solutions of either mannitol or polyethylene glycol (PEG) 6000 with osmotic potentials (π) of first −1.0 MPa and then −2.0 MPa, and the same VACs were observed after 15 min of each immersion. Images were taken at 100× magnification using a Zeiss Axiocam 208 color digital camera mounted on the light microscope.

In two further tests, TEM micrographs were obtained to verify if and how plasma membrane detachment from the cell wall (i.e. plasmolysis) occurred in the VACs (Table 1). Wood samples were either immersed in an osmotic solution ('Test 1', using a similar approach to that of the light microscopy observations) or PEG was radially injected while pressurising a stem with a pressure collar ('Test 2').

In Test 1, small (~2×1×1 mm) wood samples from the stems of potted plants were trimmed under distilled water and then placed in 1.5 ml tubes containing either distilled water (control) or a mannitol solution with a π of −2 MPa (osmotic treatment). This target π was selected because it corresponds to the leaf turgor-loss point (Ψ_{tlp}) previously reported for *P. nigra* (Blackman *et al.*, 2023). The samples were kept in open vials under vacuum for ~10 min until they sank into the solution and then the vials were sealed and kept for another 3 h at atmospheric pressure to ensure irreversible plasmolysis (the immersion time was tested using the light microscopy approach described above). Afterwards, the samples were prepared for TEM observation (see below).

Test 2 was aimed at developing a protocol for local induction of plasmolysis in VACs of stems using PEG, while concurrently inducing xylem embolism by gas injection through a pressure collar (Salleo *et al.*, 1992). The procedure allowed for subsequent hydraulic measurements on pressurised osmotically treated stems (see Experiment 1, below).

Pots were moved to the laboratory at 09.00 hand irrigated, with the shoot being covered with a black plastic bag to ensure full plant hydration. Afterwards, the bark was manually removed from a small (~60×5 mm) area of the stem at a distance of at least 30 cm from the stem base, thus exposing the wood to the air. A piece of cotton saturated with either distilled water (π=0.0 MPa) or a PEG solution (π=−3.4 MPa) was immediately placed on the debarked area and it was wrapped with Parafilm® to hold it in place and to avoid evaporation of the solution. In this case, the target π was well below the leaf Ψ_{tlp} for the species (as noted above), so the solution was expected to induce plasmolysis even allowing for some possible dilution by apoplastic water during perfusion. The stems were left with the applied patch for 1 h with the plant enclosed in a humidified black plastic bag to avoid dehydration, and then the debarked portion with the saturated cotton and Parafilm was carefully placed into a specially made double-ended chamber attached to a Digital Cavitation Chamber Instrument (PMS Instrument Company, Albany, OR, USA; see Supplementary Fig. S1). The pressure was slowly increased by a ~0.01 MPa s^{-1} until it reached 1.5 MPa and maintained for 30 min to induce embolism formation, and then it was slowly released back to atmospheric pressure.

The water-treated control ($Ctr_{1.5}$) and 1.5 MPa PEG-treated ($PEG_{1.5}$) stem portions were then used to cut small (2×1×1 mm) wood samples under 0.1 M Sørensen's phosphate buffer for TEM observations. The samples were cut from the debarked stem portions, which were likely to be the areas most affected by the applied PEG (and water) treatments. After cutting, the samples were quickly placed in 1.5 ml tubes containing the Karnovsky's fixative and prepared for TEM observations as described for Test 1 above. One sample per treatment was prepared on 4 June 2024, concurrently with the hydraulic measurements of Experiment 1 (see below). Images of 20 cells per treatment were obtained to quantify the numbers of plasmolysed cells.

Fixation and post-fixation of samples from Test 1 and Test 2 for TEM observation followed Bordenave *et al.* (2023), with some modifications, and Kaack *et al.*, 2021 for the following steps. Specifically, samples were transferred to 1 ml Karnovsky's fixative (2.5% paraformaldehyde and 0.5% glutaraldehyde in 0.1 M Sørensen's phosphate buffer) and kept for 12 h at 4 °C. However, in Test 1, in order to avoid possible deplasmolysis during fixation, the samples that had been immersed in the mannitol solution for the osmotic treatment were transferred into a mannitol-enriched Karnovsky's fixative at π of −2.0 MPa instead of the standard fixative, which has a π of −0.5 MPa. Due to initial floating, samples of Test 2 were kept under the standard Karnovsky's fixative solution using a small piece of mesh that was inserted in the tube. After removing the fixative, the samples were washed twice with 1 ml of 0.1 M Sørensen's phosphate buffer for 5 min each time. Post-fixation was performed with 1 ml of 2% OsO_4 in 0.2 M phosphate buffer (PB) for 2 h at room temperature, followed by two washes in 0.1 M PB, lasting 5 min each. This first part of the protocol was conducted at the University of Trieste, whilst the rest was conducted at Ulm University. Samples were transported between the two sites in sealed Eppendorf tubes with PB within two days, and stored for a few days before processing.

Once in Ulm, all samples were stained *en bloc* with uranyl acetate, and dehydrated through a gradual ethanol series (30%, 50%, 70%, and 90%) for 2–3 min. The samples were then embedded in Epon resin (Sigma-Aldrich) at 60 °C. Ultra-thin sections (60–80 nm) were obtained with a diamond knife using an ultra-microtome (Leica Ultracut UCT) and deposited on nickel TEM grids with a formvar/carbon coat and a 2×0.5 mm slot (Athena, Plano GmbH, Wetzlar, Germany). Observations were carried out with a JEM-1210 TEM (JEOL, Tokyo, Japan) at an accelerating voltage of 120 kV.

PEG can affect cellulose microfibril arrangement in wood cell walls (Penttilä *et al.*, 2020) and this could possibly increase pore constriction sizes of intervessel pit membranes, and consequently decrease embolism resistance (Kaack *et al.*, 2021). In order to determine whether the PEG perfusion treatments in Experiments 1 and 2 would significantly affect these properties, intervessel pit membrane thickness was quantified in the $Ctr_{1.5}$ and $PEG_{1.5}$ samples previously prepared for TEM observations of the VACs. After image acquisition, the pit membrane thickness (T_{pm}) was measured using the FiJi software (Schindelin *et al.*, 2012), based on the mean value of three measurements made at the centre of each interconduit pit membrane. Measurements were performed on 22 and 24 pit membranes for the $Ctr_{1.5}$ and $PEG_{1.5}$ samples, respectively.

Osmotic solutions

All osmotic solutions were prepared to the target value of π according to the equation presented by Michel and Kaufmann (1973) for PEG 6000 and according to the Van't Hoff equation for mannitol.

All solutions used to immerse or perfuse the wood samples (mannitol, PEG 6000, Karnowsky's fixative, buffer solutions) were then measured at ambient temperature (22 °C) using a dew-point water potential meter (WP4C, Meter Group, Inc., Pullman, WA, USA) to verify the actual π.

Experiment 1: stem pressurisation and embolism induction through a pressure collar

The xylem pressurisation procedure described above for TEM analyses in Test 2 was repeated for other stems of intact potted plants and in cut branches collected from mature trees. The aim of this experiment was to quantify the possible impact of plasmolysis on xylem vulnerability to embolism formation as induced by gas injection (Fig. 1A). The experiments on cut branches and on intact potted plants were performed from 25 May to 29 June 2023 and from 21 May to 6 June 2024, respectively.

Potted plants were treated as described in Test 2. For branches, ~1 m-long samples were cut in the evening from trees and trimmed

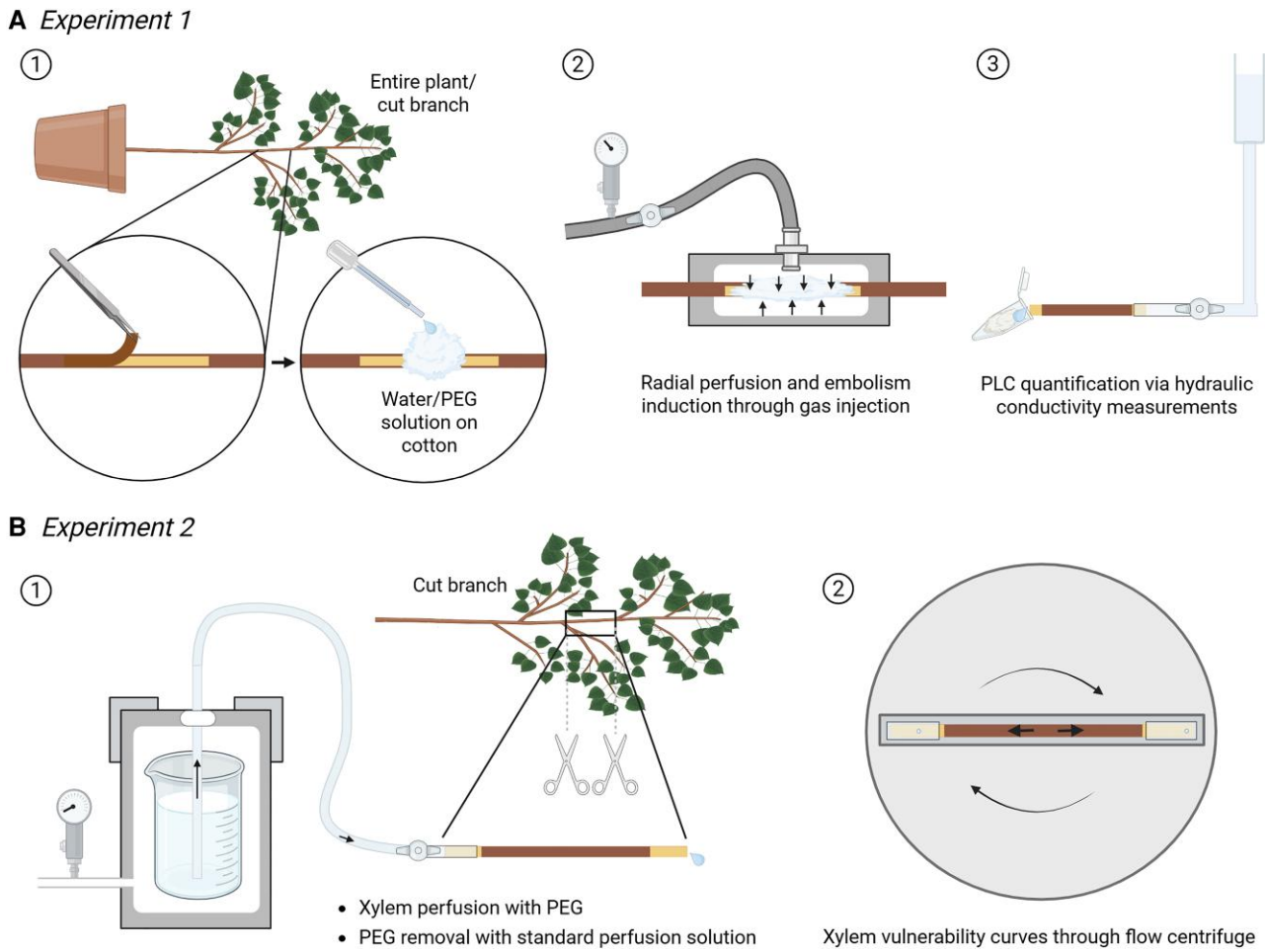

Fig. 1. Scheme of the hydraulic experiments. (A) Experiment 1. (1) A small area of bark was removed from the intact stem of a potted plant or from a branch of a tree, and a piece of cotton saturated with either water (control) or a PEG solution was positioned on it and held in place with Parafilm. (2) The sample was positioned inside a pressure collar and pressure was applied to radially perfuse the solution into the stem/branch and to induce embolism (see Supplementary Fig. S1). (3) The branch/stem was placed under water, cut, and left to achieve xylem relaxation, after which the percentage loss of hydraulic conductivity (PLC) was measured gravimetrically. (B) Experiment 2. (1) A beaker with the perfusion solution was placed inside a chamber and pressure was applied to flush the solution via a capillary tube through the xylem of a branch sampled from a tree. An initial flush with a standard solution was applied to remove possible embolisms. Control samples were then immediately used for measurements. Treated samples were next perfused first with a PEG solution and then flushed again with the standard solution before being used for measurements. (2) Measurements of hydraulic conductivity and generation of xylem vulnerability curves were carried out using a flow-centrifuge. Figure created in BioRender. Tomasella, M. (2025) https://BioRender.com/e2ktfar.

under water a few centimeters from the base. The branches were fully rehydrated overnight by covering with a plastic bag with the cut section immersed in a bucket of water. Each branch was debarked at a distance of at least 50 cm from the cut end, which was kept immersed in tap water during the whole sample preparation and pressurisation procedure. Preliminary experiments showed that branches from mature trees were more resistant to xylem embolism than stems of potted plants. Therefore, the cut branches were pressurised at 2.2 MPa while the stems of potted plants were pressurised at 1.5 MPa. After depressurisation and removal of the pressure collar, the branches were cut shorter and the stems of the potted plants were cut at the base, always under water in both cases. Consecutive cuts were made at both ends of the sample (branch or stem) until a segment of ~30 cm was obtained with the pressurised portion at the centre. The samples were kept under clean tap water for 45 min to relax internal pressure (i.e. until no gas bubbles could be seen emerging from the cut sections) then trimmed again at both ends under clean tap water to obtain a 5–6 cm-long segment, and finally cut thinly and more precisely using a sharp razor blade to leave a clean surface. The segment was then connected to a custom-made apparatus for hydraulic conductivity measurements, following Tomasella *et al.* (2019). For the perfusion solution we used filtered (0.45 μm) and degassed distilled water with KCl added at 10 mM. Stem hydraulic conductance was measured gravimetrically under a water pressure head of 3.5 kPa, before (initial hydraulic conductance, K_i) and after (maximum hydraulic conductance, K_{max}) flushing the sample at 0.15 MPa for 5 min to remove embolism. The percentage loss of hydraulic conductance (PLC) was calculated as:

$$PLC = 100 \times [1 - (K_i/K_{max})] \quad (1)$$

Branch samples treated with water or PEG solution and pressurised at 2.2 MPa were named as $Ctr_{2.2}$ and $PEG_{2.2}$, respectively. As an additional treatment, samples were prepared as described for $PEG_{1.5}$ and

$PEG_{2.2}$ but the branches or stems were pressurised at 0.5 MPa, below the pressure threshold for embolism formation in poplar (Tomasella *et al.*, 2021). This was done to exclude the possibility that the effect of the local osmotic treatment with PEG might be sufficient to generate xylem tensions that triggered embolism formation. Additional samples were measured without any pressurisation treatment or bark removal to check the native PLC of poplar branches and stems (Ctr_0). Five to seven replicates per treatment and type of sample (stems/branches) were used.

Experiment 2: xylem perfusion and quantification of vulnerability to xylem embolism with a flow centrifuge

A second experimental approach was applied at Ulm University between 25 June and 4 July 2024 to verify the effect of plasmolysis on xylem hydraulic vulnerability (Fig. 1B).

One-year-old branches ~1 m long were collected at ~08.00 h, placed in black plastic bags containing humid paper, and transported to the laboratory within 20 min. The base was recut twice under water and the branches were kept covered in the black plastic bags for ~2 h prior to sample preparation.

A branch segment ~35 cm in length without side branches was cut from within the 1-year growth portion and kept under water, and ~10 cm of bark was removed at both ends. Possible residual embolism was removed by flushing the samples with the control perfusion solution prepared with filtered, degassed deionised water containing 10 mM KCl and 1 mM $CaCl_2$ (Nardini *et al.*, 2007). A 1505D Pressure Chamber (PMS Instrument co.) was used to flush the xylem conduits as follows. The beaker containing the solution was placed inside the chamber with a capillary tube leading from it the branch outside the chamber (see Fig. 1B). A pressure of 0.15 MPa was applied for 15 min to perfuse the solution through the xylem. For the control (referred to as control flow centrifuge, Ctr_{fc}), the samples were then immediately prepared for the flow centrifuge measurements (see below). For the PEG treatment, after flushing the samples, they were then perfused with PEG 6000 with π of −3.4 MPa (PEG_{fc}; same π as used in Experiment 1) at a pressure of 0.05 MPa for 30 min, after which the ends of the branch segment where the bark had been removed were kept sealed with HDPE tubing in order to avoid gas entry and dehydration, and the samples were left for 3 h. The PEG solution was then removed by a second flush at 0.15 MPa for 5 min with the standard perfusion solution in order to ensure that no PEG-induced surface tension changes in the perfused solution could influence xylem vulnerability. PEG removal was checked by collecting the fluid exiting the sample and verifying that π was close to 0 MPa using a dew-point hygrometer. Six replicate samples were used for Ctr_{fc} and PEG_{fc}. Given that xylem vessels are in contact with VACs through pits, lowering the xylem water potential with the PEG solution should result in movement of water from VACs to the vessels, thereby decreasing the water potential of the VACs far below the turgor-loss point of *P. nigra*. Thus, we hypothesised that this treatment should induce plasmolysis equally in all the VACs.

Xylem vulnerability curves were obtained at 22 °C with a flow-centrifuge (ChinaTron, Model H2100R, Cence Company, Xiangyi, China; Wang *et al.*, 2014). After the perfusion treatments described above, the branch segments were trimmed under tap water to 27.4 cm with a sharp razor blade and inserted into the centrifuge rotor with their ends in cuvettes (Fig. 1B). The wood diameters at the cut ends of the branch segments were between 5–7 mm. The flow-centrifuge measurements of hydraulic conductivity were performed by injecting 10 mM KCl and 1 mM $CaCl_2$ in deionised water (Nardini *et al.*, 2007) into the cuvettes with a peristaltic pump (PP 2201, VWR International bvba, Leuven, Belgium). Given that the spinning time at a given rotational speed can influence the hydraulic conductivity of the sample due to gas diffusion (Silva *et al.*, 2024), measurements were conducted 5 min after reaching the target rotational speed, i.e. the time needed to get a stable flow in the centrifuge. At each rotational speed from 2000 rpm (equivalent to −0.35 MPa) to 5000 rpm (−2.20 MPa), calculated the mean value of three consecutive conductivity measurements at stable flow as obtained from the ChinaTron.

Statistical analyses

All statistical analyses were carried out using R (www.r-project.org). Box-plots were obtained with the ggplot2 package. For the T_{pm} and PLC data of Experiment 1, when assumptions of normality of residuals and homogeneity of variances were not violated, one-way ANOVA [response variable ~f(treatment)] through the aov function was used, followed by Tukey's HSD post-hoc test through the TukeyHSD function in the stats package. When data were heteroscedastic, generalised least squares (GLS) analysis was performed with the gls function with the varIdent variance structure, in the nlme R package (http://dx.doi.org/10.32614/CRAN.package.nlme), followed by Tukey's HSD test, with *P*-values adjusted using the Bonferroni–Holm method.

Vulnerability curves obtained with the ChinaTron were fitted using a Weibull function with the *fitplcs* function of the fitplc R package (Duursma and Choat, 2017), considering the individual branches as a random effect. The water potential at 50% PLC (P_{50}) and the associated 95% confidence intervals (CIs) were calculated as output of the model. Significant differences between Ctr_{fc} and PEG_{fc} curves were determined based on the absence of CI overlap.

Results

Light microscopy *in vitro* observations of plasmolysis

Vacuole staining with Neutral Red allowed us to visualise wood parenchyma of *P. nigra* and to identify intact VACs (Fig. 2; Supplementary Fig. S2). It should be noted that VACs in *P. nigra* are only ray cells because this species lacks axial parenchyma. Therefore, under light microscopy, intact VACs often appeared in a layer immediately below the vessels, with wide vessel–parenchyma pits grouped in dense pit fields. When immersed in the buffer at π=−0.2 MPa, a single, large vacuole was observed and, as expected, it seemed to occupy almost the entire protoplast volume (Fig. 2A, B; Supplementary Fig. S2A). Immersion of the radial sections in PEG or mannitol solutions at progressively lower π induced protoplast shrinkage, as clearly indicated by the progressive reduction of the vacuole volume. For both solutions, a concave plasmolysis was observed, possibly indicating that the plasma membranes were strongly bound to cell walls (Oparka, 1994). At any given π, plasma membrane detachment from cell walls was more pronounced when the samples were immersed in the PEG than in the mannitol solution.

TEM observations

In Test 1, the immersion of the wood in the mannitol solution at π=−2.0 MPa (osmotic treatment) induced clear plasmolysis in most of the observed VACs (18 out of 20), with partial (in most cases) or apparently total detachment of the plasma membrane from the cell wall, forming gaps that appeared frequently at the vessel–parenchyma pit membrane interface (Fig. 3E–H). All the observed VACs (n=20) in the corresponding control

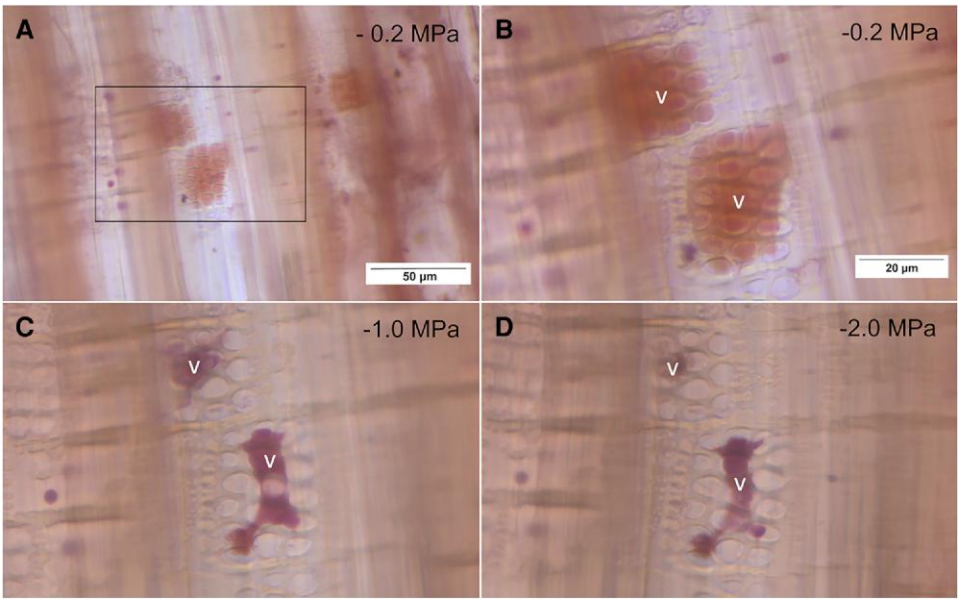

Fig. 2. Light microscope images of plasmolysis of vessel-associated parenchyma cells. In the Preliminary Test, stem radial sections of *P. nigra* were stained with Neutral Red in a buffer solution and then treated with PEG solutions at progressively decreasing osmotic potentials. (A) Section treated with the buffer solution at –0.2 MPa and (B) a close-up of the area highlighted in (A). (C) The same cells at 15 min after treatment with PEG solution at –1.0 MPa, followed by (D) treatment with PEG at –2.0 MPa. 'v, indicates vacuoles stained with Neutral Red.

treatment (i.e. immersed in water) appeared intact and turgid, with often a single large vacuole (more rarely two) in the central region of the protoplast, and plasma membranes in contact with cell walls (Fig. 3A–D).

The pressurisation experiment with a PEG solution at π= −1.5 MPa (Test 2, $PEG_{1.5}$) showed a high number of VACs with partially detached plasma membranes (12 out of 20; Fig. 3M–P), in comparison with control samples treated with water (only two cells with detached membranes out of 20; Fig. 3I–L). In general, vacuoles were visible and large only in intact non-plasmolysed cells.

Intervessel pit-membrane thickness did not differ between the water- and PEG-treated samples of Experiment 1 (P=0.532), with mean (±SD) values of 228±61 nm and 239 ±59 nm, respectively.

Experiment 1: xylem pressurisation and gas injection with a pressure collar

The mean PLC of branches treated with PEG solution and pressurised at 0.5 MPa ($PEG_{0.5}$) was 5%, and did not significantly differ from that of control branches that were untreated and not pressurised (Ctr_0, 11%; Fig. 4A). PEG treatment of branches pressurised at 2.2 MPa induced an increase of mean PLC up to ~80%, which was about double the values recorded for branches exposed to the same pressure but treated with water ($Ctr_{2.2}$, PLC=41%; P=0.002). Similar results were obtained in the pressurisation experiment conducted on the stems of potted plants (Fig. 4B). In this case, the mean PLC of the $PEG_{0.5}$ samples was ~13%, and did not differ from that of the Ctr_0 samples (9%). The PLC of stems pressurised at 1.5 MPa was significantly higher in the PEG-treated ($PEG_{1.5}$, 68%) than in the water-treated ($Ctr_{1.5}$, 44%) samples (P=0.005).

Experiment 2: xylem perfusion and xylem vulnerability to embolism

The xylem water potential inducing 50% loss of hydraulic conductivity (P_{50}) of the control samples flushed with the standard perfusion solution (Ctr_{fc}) was −1.42 MPa (lower and upper CI of −1.41 MPa and −1.44 MPa, respectively; Fig. 5). The PEG-perfused samples (PEG_{fc}) showed a significant shift in the xylem vulnerability curve compared with the Ctr_{fc} samples, with increased vulnerability and less-negative P_{50} values, averaging −1.29 MPa (lower and upper CI of −1.28 MPa and −1.31 MPa, respectively).

Discussion

In this study, we aimed at verifying the hypothesis that loss of turgor and consequent plasmolysis of vessel-associated parenchyma cells might generate gas-filled gaps between the plasma membrane and the cell wall/vessel–parenchyma pits. We hypothesised that this gas volume might represent a trigger for gas propagation into the adjacent conduit, thus increasing xylem vulnerability to embolism formation. In this perspective, the porous vessel–parenchyma pit membranes would function

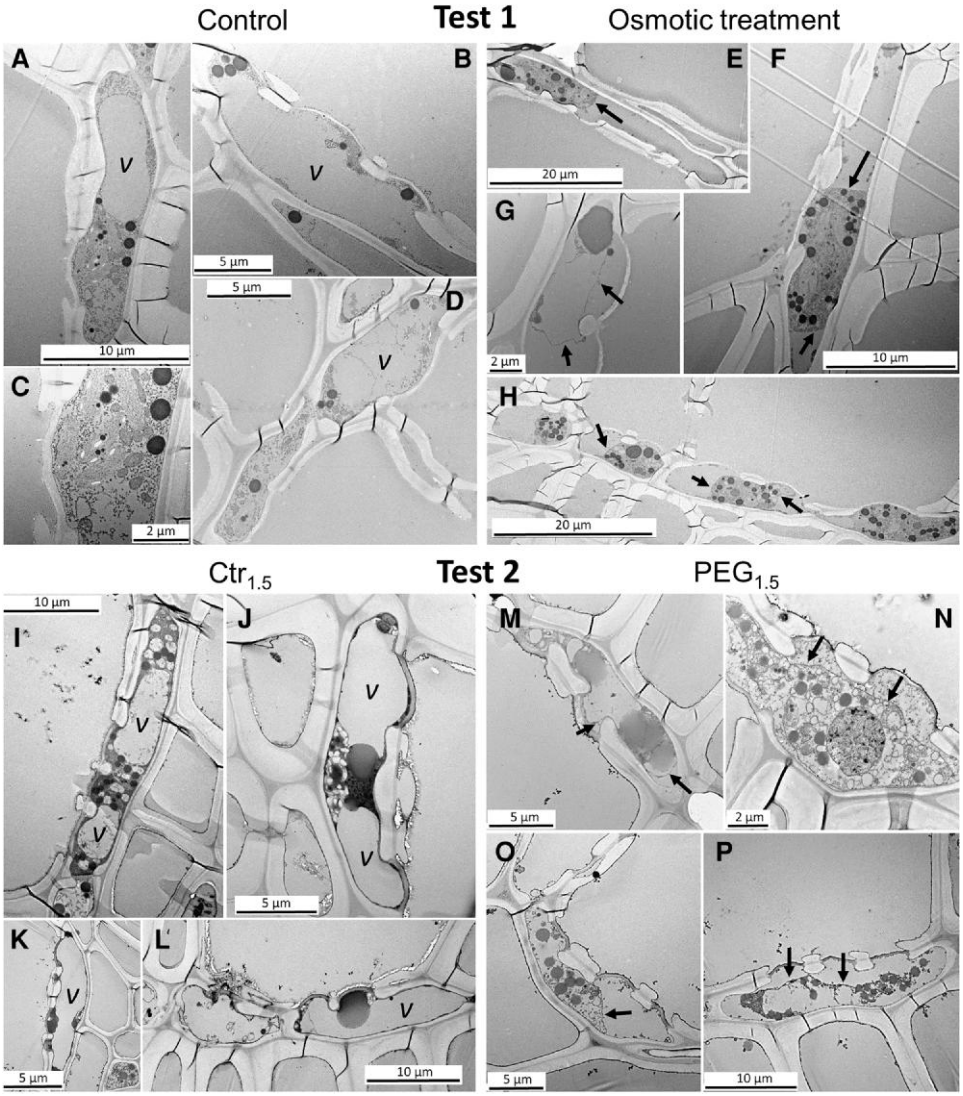

Fig. 3. TEM images of vessel-associated parenchyma cells (VACs) and their vessel–parenchyma pits in *P. nigra* wood following different test treatments with mannitol or PEG solutions. (A–H) In Test 1, small wood samples from a potted plant were immersed either in buffer solution (control, A–D) or in mannitol solution with an osmotic potential of –2 MPa (osmotic treatment, E–H). The image in (C) shows a magnified detail of (A). (I–P) In Test 2, a small area of bark was removed from the stem, a piece of cotton was applied saturated with either water ($Ctr_{1.5}$, I–L) or a PEG solution at –3.4 MPa ($PEG_{1.5}$, M–P), and then the stem was pressurised to 1.5 MPa inside a pressure collar (see Fig. 1A; Supplementary Fig. S1). Representative images at different magnification. Arrows indicate plasma membrane detachment in osmotically treated samples, and 'v' indicates large vacuoles in VACs.

similar to intervessel pit membranes between an embolised and a water-filled vessel, leading to embolism in the previously functional vessels. Our results supported the experimental hypothesis by showing first that upon turgor loss, plasmolysis could occur in VACs of *P. nigra* stems, and second that this was associated with an increased vulnerability to xylem embolism, thus showing a possible mechanistic linkage between turgor loss and embolism build-up.

In order to maintain plant hydration and functionality at decreasing water potentials, an osmotically driven decrease in Ψ_{tlp} is typically observed across the growing season at mid-latitudes, and in general during the progression of a period of drought and heat (e.g. Feng *et al.*, 2023). Accordingly, progressive accumulation of sugars for osmoregulation and related depletion of starch in the wood are also commonly observed during drought (e.g. Tomasella *et al.*, 2019, 2020; He *et al.*, 2020). On the other hand, depletion of NSCs can impair this capability of osmoregulation (Sevanto *et al.*, 2014; Sapes *et al.*, 2021). Starch reserves are a major source of sugars under drought and their marked depletion or limited accessibility during drought is associated with substantial loss of hydraulic integrity (Trueba *et al.*, 2024). In addition, several studies have shown evidence

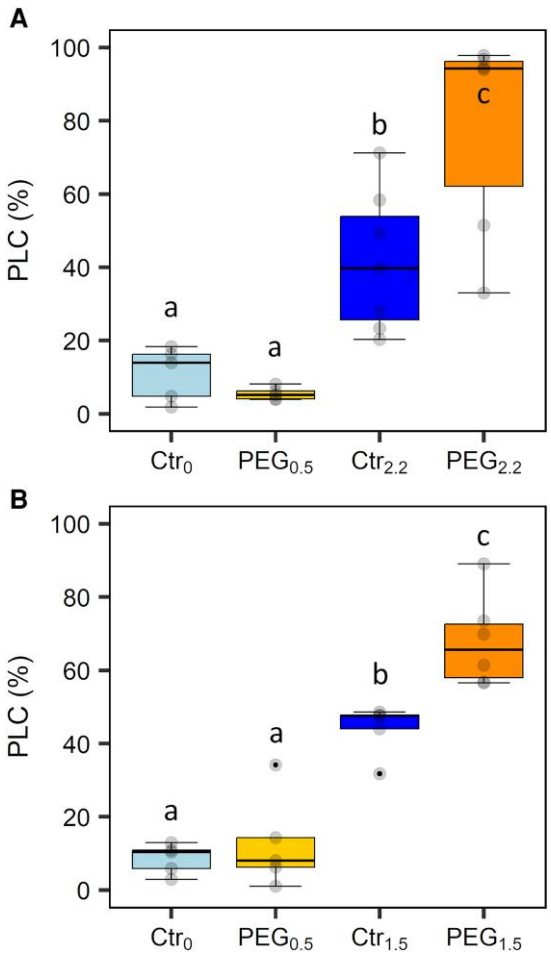

Fig. 4. Percentage loss of xylem hydraulic conductance (PLC) in *P. nigra* branches of (A) mature trees and (B) stems of potted plants subjected to different osmotic and pressurisation treatments in Experiment 1. PLC was measured in non-treated control samples (Ctr_0), in samples treated with water and pressurised at either 2.2 MPa ($Ctr_{2.2}$) or 1.5 ($Ctr_{1.5}$), and in samples treated with a PEG solution at −3.4 MPa and then pressurised to 0.5 MPa ($PEG_{0.5}$), to 2.2 MPa ($PEG_{2.2}$), or to 1.5 MPa ($PEG_{1.5}$) (see Fig. 1A; Supplementary Fig. S1). The line within the box, the box margins, and the whiskers represent the median, the interquartile range, and the minimum and maximum non-outlier values, respectively. Gray dots are individual data points and the small black dots indicate outliers. Different letters indicate significant differences among treatments ($P<0.05$) as determined using generalised least squares analysis in (A) where the data were heteroscedastic, and using one-way ANOVA followed by Tukey's HSD test in (B).

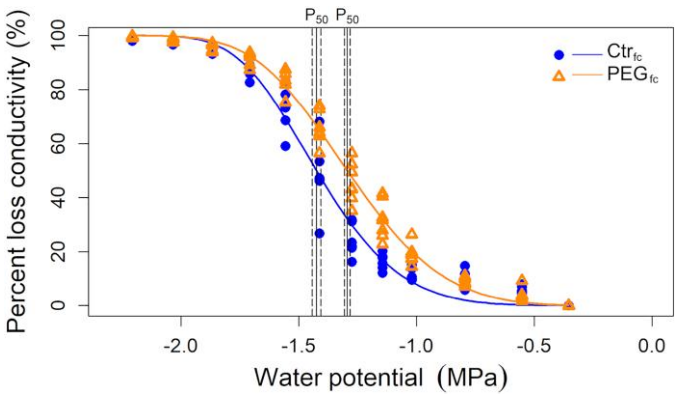

Fig. 5. Xylem vulnerability curves obtained for *P. nigra* branches using the flow-centrifuge technique in Experiment 2. Branches from mature trees were perfused either with a control solution (Ctr_{fc}) or a PEG solution (PEG_{fc}) at an osmotic potential of −3.4 MPa and then xylem vulnerability curves were obtained using a flow-centrifuge instrument (Fig. 1A; see Methods for details). The water potential at 50% loss of xylem hydraulic conductivity (P_{50}) is indicated for each curve, where the dashed lines indicate the 95% confidence intervals (n=6).

that NSC-depleted plants become more vulnerable to drought-induced embolism (De Baerdemaeker *et al.*, 2017; Tomasella *et al.*, 2021) and/or are susceptible to earlier mortality (e.g. O'Brien *et al.*, 2014). In general, hydraulic failure is often accompanied by NSC depletion in trees under drought, suggesting an interrelation between the two processes (McDowell *et al.*, 2011; Adams *et al.*, 2017). Considering this evidence together with the results of our current study, we suggest that hindered osmoregulation due to drought-induced NSC depletion could cause earlier turgor loss in VACs, which in turn would increase the risk of xylem embolism.

The patterns of plasma membrane detachment following osmotically induced turgor loss were assessed in stem VACs) through light and transmission electron microscopy (Figs 2, 3). In particular, the TEM observations of wood samples subjected to PEG treatment and gas injection confirmed that many VACs were indeed plasmolysed after the pressurisation at 1.5 MPa, whereas most of VACs maintained turgor in the control samples treated with water. We noted a lower fraction of plasmolysed VACs in Test 2 than in Test 1. This was likely to be due to the different methods used to deliver the osmotic solution to the samples, as PEG was injected radially from the outer xylem surface through pressurisation in Test 1, whereas small wood samples were completely immersed in the osmotic solution in Test 2, which probably allowed most of the VACs to come into contact with the solution.

Gaps between the detached plasma membrane and the vessel–parenchyma pit membranes could represent a preferential gas source for the build-up of embolism. Indeed, plasma membrane retraction from cell walls, clearly seen in the TEM images of PEG-treated samples, created voids at the vessel–parenchyma pit interface (Fig. 3). It is likely that the apoplastic spaces between the plasma membrane and cell wall become filled with gas at atmospheric pressure as intercellular spaces are in equilibrium with atmospheric gas outside the plant. We highlight that in our tests plasmolysis was artificially induced: future studies, perhaps carried out through *in vivo* imaging techniques such as X-ray micro- or nano-tomography on, for example, NSC-depleted plants (which would show a lower or hindered osmoregulation capacity), could verify the occurrence of gas-filled spaces and clarify under what conditions plasmolysis of VACs might occur under drought in field conditions.

In this study, we used different approaches for inducing plasmolysis and different methods to induce and assess xylem

embolism in *P. nigra* stems. These multiple approaches were useful for excluding possible method-related biases, which could compromise the results. We observed good agreement among the methods and an overall convergence in the findings. In particular, using a classic hydraulic apparatus we were able to verify an increase in PLC upon PEG treatment and gas injection, both in cut branches and in intact potted plants (Fig. 4). The same effect was observed when assessing xylem vulnerability with a flow-centrifuge after a perfusion treatment with PEG using branches. Stems of potted plants measured with the hydraulic method after gas injection, and branches from trees measured with the flow-centrifuge technique both showed similar xylem vulnerability, as the PLC of stems pressurised at 1.5 MPa was 44% and the P_{50} of the Ctr_{fc} samples was −1.42 MPa. These results are in line with vulnerability curves previously obtained for *P. nigra* by dehydration of entire potted plants and quantification of PLC with classic hydraulic and optical methods (Tomasella *et al.*, 2021). On the other hand, branches of mature trees treated using a pressure collar appeared to be more resistant, because PLC was still around 41% when pressurised at 2.2 MPa. This higher resistance in mature trees could be the result of ontogeny and drought acclimation, given that the trees sampled were growing in a parking lot and probably had low below-ground water availability, especially in summer (Savi *et al.*, 2015). In addition, the osmotic treatment produced a stronger increase in PLC (by ∼40%) in branches from mature trees pressurised with a pressure collar ($PEG_{2.2}$) compared with stems of potted plants and of branches measured with the ChinaTron, in which PLC increased by ∼20% (from 50% to 70%) at water potentials of about −1.4 MPa (Fig. 5).

PEG 6000 is often used to induce osmotic stress in plant cells as well at the root-system level (Hohl and Schopfer, 1991; Peralta Ogorek *et al.*, 2024); however, PEG with molecular weights between 300–4000 g mol^{-1} has been shown to interact with cellulose microfibrils of wood-cell walls, increasing their packing and decreasing interfibrillar distance (Penttilä *et al.*, 2020). If pit membranes shrink due to PEG infiltration, it could be assumed that the pore-volume fraction would decrease upon PEG treatment and most of the pores in the pit membrane would become smaller; however, a few wide pores could also form by re-arrangement of cellulose microfibrils, possibly affecting the xylem vulnerability to embolism (Kaack *et al.*, 2019). Under this scenario, pit membranes would be expected to become thinner (a phenomenon commonly observed during dehydration; Jansen *et al.*, 2008). However, the $Ctr_{1.5}$ and $PEG_{1.5}$ samples did not differ in terms of intervessel pit-membrane thickness, so we are confident in excluding the occurrence of this phenomenon and its related effects in our experiments.

The half-bordered vessel–parenchyma pits were relatively wide (Fig. 3), as commonly observed in many species (e.g. van Bel, 1990). This indicated that the surface area for exchange of water, ions, and other molecules (including gases) between the xylem vessels and the surrounding living parenchyma was rather large. Therefore, gas propagation rates through the porous pit membranes upon VAC plasmolysis would also potentially increase with increased pit size. We can assume that this process and the magnitude of its contribution to xylem embolism formation might depend on some species-specific anatomical traits, such as total vessel–parenchyma pit membrane surface areas and the vessel–VAC contact fraction. In this respect, *P. nigra* lacks axial parenchyma but vessels are well connected to parenchyma ray cells (Tomasella *et al.*, 2021). The total wood parenchyma fraction correlates with P_{50} in angiosperms, which indeed have a much higher proportion of living cells and are on average more vulnerable to xylem embolism than gymnosperms (Kiorapostolou *et al.*, 2019). Connected with this, the proportion of wood parenchyma is a major determinant of wood density in angiosperms, with softer wood having a higher parenchyma fraction (Kiorapostolou *et al.*, 2019; Trifilò *et al.*, 2019), and wood density is often correlated with xylem hydraulic vulnerability, with softer woods generally being more vulnerable to embolism under drought (Nardini *et al.*, 2013; Trifilò *et al.*, 2015). Therefore, we might hypothesise that a denser wood could be hydraulically safer because of the lower number of conduit–parenchyma contact points, which would ensure a lower risk of embolism build-up through vessel–parenchyma pit membranes upon drought-induced turgor loss and plasmolysis. Similarly, the role of turgor loss in VACs as a trigger for embolism formation might provide an additional or alternative explanation for the relationship between conduit size and vulnerability to embolism. Large conduits have frequently been reported to be hydraulically more vulnerable (Isasa *et al.*, 2023), and this has been attributed to their larger wall surface area leading to higher intervessel pit area (Wheeler *et al.*, 2005; Hacke *et al.*, 2006). In woody angiosperms an increase in vessel diameter is associated with a higher number of VACs (Morris *et al.*, 2018a). Based on these findings, it would be interesting to determine whether long and large conduits might also have more direct contacts (e.g larger vessel–parenchyma pit membrane fractions) with VACs, increasing the probability that some of these living cells undergo plasmolysis under drought stress, thus generating the gas phase responsible for conduit embolisation. Micro-CT observations of vessel- and tracheid-bearing plants have also revealed the occasional presence of isolated, embolised conduits, suggesting that in this case mechanisms other than interconduit gas propagation could trigger embolism formation (Choat *et al.*, 2016). In this respect, it would be interesting to investigate whether induced plasmolysis in VACs could be associated with different patterns of embolism formation, for example the presence of isolated embolised conduits instead of 'classical' radial patterns along neighbouring conduits.

The structure and composition of vessel–parenchyma pit membranes are similar to those of intervessel pit membranes, albeit the former contain pectins (e.g. Plavcovà and Hacke, 2011;

Kaack *et al.*, 2019), which might contribute to maintain hydration. There is also evidence that these membranes might undergo seasonal lignification (Morris *et al.*, 2018b), meaning that gas permeability might decrease as wood ages, and therefore VAC plasmolysis might be less effective for embolism spread in the late growing season or in older wood. Considering this, we can also speculate that the increasing resistance to xylem embolism documented in several species during seasonal drought progression might be the result of changes not only of xylem conduit properties (e.g. Sorek *et al.*, 2021) but also of vessel–parenchyma pit membranes and of adjustment of Ψ_{tlp} in VACs.

While our results offer a possible mechanistic interpretation of reported correlations between species-specific P_{50} and Ψ_{tlp} (Bartlett *et al.*, 2016; Christoffersen *et al.*, 2016; Chen *et al.*, 2021; De Guzman *et al.*, 2021), the progressive breakdown of this correlation for highly drought tolerant species (Martin-StPaul *et al.*, 2017) leads to additional questions and hypotheses. We propose three possible explanations for the divergence of this relationship when $P_{50}<-5$ MPa. First, as noted above, the parenchyma tissue fraction, its arrangement, and its quantitative characteristics could play an important role. Indeed, drought-tolerant species are often characterised by high wood density coupled with a low parenchyma tissue fraction, which might decrease the number of parenchyma–vessel contacts, thus reducing the likelihood that the occurrence of turgor loss could trigger or contribute to initial embolism events.

A second explanation relates to the actual occurrence of plasmolysis upon turgor loss. Previous studies (e.g. Ding *et al.*, 2014; Yang *et al.*, 2017; Schönbeck *et al.*, 2025) have suggested that turgor loss does not always coincide with the onset of plasmolysis in drought-adapted species characterised by small-sized parenchyma cells. In these species (notably those with the most negative P_{50}), negative turgor pressures might develop, preventing the detachment of the plasma membrane from the cell wall and most likely avoiding the formation of air gaps that could trigger initial embolism events.

A third important point is that our turgor-loss hypothesis might explain the initial formation of embolism events, but not the vessel-to-vessel propagation of embolism, which is most likely limited by features different from Ψ_{tlp}, such as vessel connectivity and intervessel pit-membrane characteristics. Indeed, in the scenario we propose, Ψ_{tlp} is more likely related to the gas-entry xylem-pressure threshold (P_e, indicating formation of first embolism events) rather than to P_{50} (related to a substantial spread of embolism in the vessel network). In drought-vulnerable species such as *P. nigra*, typically characterised by a steep vulnerability curve, the P_e and P_{50} values are quite close to each other (Meinzer *et al.*, 2009). In contrast, in drought-tolerant species with vulnerability curves characterised by more gentle slopes, the difference between P_e and P_{50} can be very large (up to 4 MPa; Meinzer *et al.*, 2009), leading to progressive decoupling of P_{50} from Ψ_{tlp}. To solve this issue, future analyses should focus on the possible relationship between Ψ at the onset of embolism (conventionally Ψ at 12% PLC, namely P_{12}) and Ψ_{tlp} of vessel-associated cells across species with different levels of drought tolerance.

Conclusion

Our results suggest the existence of a mechanistic link between turgor maintenance in VACs and vulnerability to xylem embolism. Moreover, this study highlights several key points that deserve further investigation. First, our hypotheses could be further supported by an assessment of the spatial patterns of embolism formation when plasmolysis is induced or occurs in VAC. Second, as we have shown that VACs could be possible trigger-points for embolism, the relationship between conduit–parenchyma pit characteristics and xylem embolism initiation/propagation should be investigated. This relationship might depend on species-specific anatomical traits related to the connectivity between wood parenchyma and xylem conduits, but also on species-specific values of Ψ_{tlp} and on the plasticity in osmoregulation, although this seems to be relatively limited (0.44 MPa variation in leaves on average; Bartlett *et al.*, 2014). In this respect, highly embolism-resistant species that diverge from the general correlation between P_{50} and Ψ_{tlp} might have evolved fewer and smaller wood parenchyma cells, and/or parenchyma cells that develop negative turgor pressure to reduce the risk of initial embolism formation even under severe water shortage.

Finally, and most importantly, considering the role of NSC availability in maintaining cell turgor during drought, NSC reserves might be involved in shaping plant hydraulic behaviour and survival under prolonged drought via maintenance of cell turgor in the VACs. If osmoregulation is impaired under drought due to NSC depletion, turgor loss would occur at less-negative water potentials than in plants with optimal NSC levels (Sapes *et al.*, 2021), possibly triggering earlier embolism formation (Tomasella *et al.*, 2021). Indeed, considering the pervasive evidence that hydraulic failure often co-occurs with NSC depletion (Adams *et al.*, 2017), our findings could provide a mechanistic explanation for the link between the two processes.

It should be noted that for hydraulically vulnerable species such as *P. nigra*, a relatively small change in water potential that triggers embolism due to limited osmoregulation, coupled with a steep slope of the vulnerability curve, might have limited impacts on the timing of damage during a drought event. However, there are several species where large seasonal variations in Ψ_{tlp}, coupled with gentler slopes of the vulnerability curve, might lead to important consequences for the potential timing and effect on embolism formation. This is the case of some Mediterranean species in which Ψ_{tlp} can decrease by even more than 1 MPa across the growing season. As an example, in *Pinus halepensis* Feng *et al.* (2023) reported a shift in Ψ_{tlp} from −2.0 MPa to −3.5 MPa from March to October,

coupled with a change in P_{50} from −2.7 MPa to −3.9 MPa. Nardini *et al.* (2003) also reported large shifts in Ψ_{tlp} from May to September for three woody species: from −2.2 MPa to −3.0 MPa in *Cotinus coggygria*, from −2.5 MPa to −3.3 MPa in *Prunus mahaleb*, and from −2.1 MPa to −3.5 MPa in *Fraxinus ornus*. In all these cases, these adjustments in Ψ_{tlp}, when translating into parallel shifts of P_e, could potentially lead to a substantial delay in the onset of xylem embolism during summer drought, thus affecting the trajectory leading to the risk of plant death by hydraulic failure.

Supplementary data

The following supplementary data are available at *JXB* online.

Fig. S1. The set-up for branch/stem pressurization with a pressure collar in Experiment 1.

Fig. S2. Light microscopy images of plasmolysis in VACs on radial sections treated with mannitol solutions.

Acknowledgements

We thank the 'Direzione centrale risorse agroalimentari, forestali e ittiche —area foreste e territorio' of the 'Regione autonoma Friuli Venezia Giulia' and the public nursery Vivai Pascul (Tarcento, Italy) for providing the potted plants used for the experiments. We thank Andrea Huppenberger (Ulm University) for her help with sample preparation and TEM observations.

Author contributions

MT and AN planned and designed the research, with contributions from SJ for experiments conducted in Ulm; MT performed the hydraulic experiments with help from CG; MT and EB performed fixation and post-fixation of samples for TEM; SJ performed TEM image acquisition; MT analysed the data and prepared the figures; MT and AN wrote the first draft of the manuscript; All authors contributed to revision of the manuscript .

Conflict of interest

The authors declare that they have no conflicts of interest in relation to this work.

Funding

This work was supported by a Microgrant 2023/2024 financed by the Regione Autonoma Friuli Venezia Giulia to MT, by the Deutscher Akademischer Austauschdienst (DAAD, Funding programme no. 57693448 'Research Stays for University Academics and Scientists, 2024') to MT for the research at Ulm University, and by the Deutsche Forschungsgemeinschaft (DFG, German Research Foundation; project no. 457287575) to SJ.

Data availability

The data supporting the findings of this study are available from the corresponding author, Martina Tomasella, upon request.

References

Adams HD, Zeppel MJB, Anderegg WRL, *et al.* 2017. A multi-species synthesis of physiological mechanisms in drought-induced tree mortality. Nature Ecology & Evolution **1**, 1285–1291.

Anderegg WRL, Berry JA, Smith DD, Sperry JS, Anderegg LDL, Field CB. 2012. The roles of hydraulic and carbon stress in a widespread climate-induced forest die-off. Proceedings of the National Academy of Sciences, USA **109**, 233–237.

Avila RT, Kane CN, Batz TA, Trabi C, Damatta FM, Jansen S, McAdam SAM. 2023. The relative area of vessels in xylem correlates with stem embolism resistance within and between genera. Tree Physiology **43**, 75–87.

Bartlett MK, Zhang Y, Kreidler N, Sun S, Ardy R, Cao K, Sack L. 2014. Global analysis of plasticity in turgor loss point, a key drought tolerance trait. Ecology Letters **17**, 1580–1590.

Bartlett MK, Klein T, Jansen S, Choat B, Sack L. 2016. The correlations and sequence of plant stomatal, hydraulic, and wilting responses to drought. Proceedings of the National Academy of Sciences, USA **113**, 13098–13103.

Blackman CJ, Billon LM, Cartailler J, Torres-Ruiz JM, Cochard H. 2023. Key hydraulic traits control the dynamics of plant dehydration in four contrasting tree species during drought. Tree Physiology **43**, 1772–1783.

Bloemen J, Vergeynst LL, Overlaet-Michiels L, Steppe K. 2016. How important is woody tissue photosynthesis in poplar during drought stress? Trees **30**, 63–72.

Blum A. 2017. Osmotic adjustment is a prime drought stress adaptive engine in support of plant production: osmotic adjustment and plant production. Plant, Cell & Environment **40**, 4–10.

Bordenave CD, García-Breijo F, Gazquez A, Muggia L, Carrasco P, Barreno E. 2023. Low temperature scanning electron microscopy (LTSEM) findings on the ultrastructure of *Trebouxia lynnae* (Trebouxiophyceae, lichenized microalgae). Diversity **15**, 170.

Brodersen CR, McElrone AJ, Choat B, Lee EF, Shackel KA, Matthews MA. 2013. *In vivo* visualizations of drought-induced embolism spread in *Vitis vinifera*. Plant Physiology **161**, 1820–1829.

Charrier G, Delzon S, Domec JC, *et al.* 2018. Drought will not leave your glass empty: low risk of hydraulic failure revealed by long-term drought observations in world's top wine regions. Science Advances **4**, eaao6969.

Chen Z, Zhang Y, Yuan W, Zhu S, Pan R, Wan X, Liu S. 2021. Coordinated variation in stem and leaf functional traits of temperate broadleaf tree species in the isohydric–anisohydric spectrum. Tree Physiology **41**, 1601–1610.

Choat B, Lahr EC, Melcher PJ, Zwieniecki MA, Holbrook NM. 2005. The spatial pattern of air seeding thresholds in mature sugar maple trees. Plant, Cell & Environment **28**, 1082–1089.

Choat B, Jansen S, Brodribb TJ, *et al.* 2012. Global convergence in the vulnerability of forests to drought. Nature **491**, 752–755.

Choat B, Badel E, Burlett R, Delzon S, Cochard H, Jansen S. 2016. Noninvasive measurement of vulnerability to drought-induced embolism by X-ray microtomography. Plant Physiology **170**, 273–282.

Christoffersen BO, Gloor M, Fauset S, *et al.* 2016. Linking hydraulic traits to tropical forest function in a size-structured and trait-driven model (TFS v.1-Hydro). Geoscientific Model Development **9**, 4227–4255.

Cochard H, Cruiziat P, Tyree MT. 1992. Use of positive pressures to establish vulnerability curves: further support for the air-seeding hypothesis and implications for pressure–volume analysis. Plant Physiology **100**, 205–209.

De Baerdemaeker NJF, Salomón RL, De Roo L, Steppe K. 2017. Sugars from woody tissue photosynthesis reduce xylem vulnerability to cavitation. New Phytologist **216**, 720–727.

De Guzman ME, Acosta-Rangel A, Winter K, Meinzer FC, Bonal D, Santiago LS. 2021. Hydraulic traits of Neotropical canopy liana and tree species across a broad range of wood density: implications for predicting drought mortality with models. Tree Physiology **41**, 24–34.

Dietze MC, Sala A, Carbone MS, Czimczik CI, Mantooth JA, Richardson AD, Vargas R. 2014. Nonstructural carbon in woody plants. Annual Review of Plant Biology **65**, 667–687.

Ding Y, Zhang Y, Zheng Q-S, Tyree MT. 2014. Pressure–volume curves: revisiting the impact of negative turgor during cell collapse by literature review and simulations of cell micromechanics. New Phytologist **203**, 378–387.

Duursma R, Choat B. 2017. Fitplc – an R package to fit hydraulic vulnerability curves. The Journal of Plant Hydraulics **4**, e002.

Enns LC, Canny MJ, McCully ME. 2000. An investigation of the role of solutes in the xylem sap and in the xylem parenchyma as the source of root pressure. Protoplasma **211**, 183–197.

Feng F, Wagner Y, Klein T, Hochberg U. 2023. Xylem resistance to cavitation increases during summer in *Pinus halepensis*. Plant, Cell & Environment **46**, 1849–1859.

Guan X, Pereira L, McAdam SAM, Cao K, Jansen S. 2021. No gas source, no problem: proximity to pre-existing embolism and segmentation affect embolism spreading in angiosperm xylem by gas diffusion. Plant, Cell & Environment **44**, 1329–1345.

Hacke UG, Sperry JS, Wheeler JK, Castro L. 2006. Scaling of angiosperm xylem structure with safety and efficiency. Tree Physiology **26**, 689–701.

Hartmann H, Trumbore S. 2016. Understanding the roles of nonstructural carbohydrates in forest trees – from what we can measure to what we want to know. New Phytologist **211**, 386–403.

He W, Liu H, Qi Y, Liu F, Zhu X. 2020. Patterns in nonstructural carbohydrate contents at the tree organ level in response to drought duration. Global Change Biology **26**, 3627–3638.

Hohl M, Schopfer P. 1991. Water relations of growing maize coleoptiles: comparison between mannitol and polyethylene glycol 6000 as external osmotica for adjusting turgor pressure. Plant Physiology **95**, 716–722.

Isasa E, Link RM, Jansen S, Tezeh FR, Kaack L, Sarmento Cabral J, Schuldt B. 2023. Addressing controversies in the xylem embolism resistance–vessel diameter relationship. New Phytologist **238**, 283–296.

Jacobsen AL, Pratt RB, Davis SD, Ewers FW. 2007. Cavitation resistance and seasonal hydraulics differ among three arid Californian plant communities. Plant, Cell & Environment **30**, 1599–1609.

Jansen S, Pletsers A, Sano Y. 2008. The effect of preparation techniques on SEM-imaging of pit membranes. IAWA Journal **29**, 161–178.

Jansen S, Choat B, Pletsers A. 2009. Morphological variation of intervessel pit membranes and implications to xylem function in angiosperms. American Journal of Botany **96**, 409–419.

Kaack L, Altaner CM, Carmesin C, *et al.* 2019. Function and three-dimensional structure of intervessel pit membranes in angiosperms: a review. IAWA Journal **40**, 673–702.

Kaack L, Weber M, Isasa E, *et al.* 2021. Pore constrictions in intervessel pit membranes provide a mechanistic explanation for xylem embolism resistance in angiosperms. New Phytologist **230**, 1829–1843.

Kiorapostolou N, Da Sois L, Petruzzellis F, Savi T, Trifilò P, Nardini A, Petit G. 2019. Vulnerability to xylem embolism correlates to wood parenchyma fraction in angiosperms but not in gymnosperms. Tree Physiology **39**, 1675–1684.

Klepsch MM, Schmitt M, Knox JP, Jansen S. 2016. The chemical identity of intervessel pit membranes in *Acer* challenges hydrogel control of xylem hydraulic conductivity. AoB Plants **8**, plw052.

Lens F, Sperry JS, Christman MA, Choat B, Rabaey D, Jansen S. 2011. Testing hypotheses that link wood anatomy to cavitation resistance and hydraulic conductivity in the genus *Acer*. New Phytologist **190**, 709–723.

Li S, Lens F, Espino S, Karimi Z, Klepsch M, Schenk HJ, Schmitt M, Schuldt B, Jansen S. 2016. Intervessel pit membrane thickness as a key determinant of embolism resistance in angiosperm xylem. IAWA Journal **37**, 152–171.

Ma BL, Liao SH, Lv QZ, Huang X, Jiang ZM, Cai J. 2024. Seasonal plasticity of stem embolism resistance and its potential driving factors in six temperate woody species. Physiologia Plantarum **176**, e14421.

Maherali H, Pockman WT, Jackson RB. 2004. Adaptive variation in the vulnerability of woody plants to xylem cavitation. Ecology **85**, 2184–2199.

Martin-StPaul N, Delzon S, Cochard H. 2017. Plant resistance to drought depends on timely stomatal closure. Ecology Letters **20**, 1437–1447.

McDowell NG, Beerling DJ, Breshears DD, Fisher RA, Raffa KF, Stitt M. 2011. The interdependence of mechanisms underlying climate-driven vegetation mortality. Trends in Ecology & Evolution **26**, 523–532.

Meinzer FC, Johnson DM, Lachenbruch B, McCulloh KA, Woodruff DR. 2009. Xylem hydraulic safety margins in woody plants: coordination of stomatal control of xylem tension with hydraulic capacitance. Functional Ecology **23**, 922–930.

Michel BE, Kaufmann MR. 1973. The osmotic potential of polyethylene glycol 6000. Plant Physiology **51**, 914–916.

Moreno M, Limousin JM, Simioni G, *et al.* 2024. Hydraulic plasticity and water use regulation act to maintain the hydraulic safety margins of Mediterranean trees in rainfall exclusion experiments. Plant, Cell & Environment **47**, 4741–4753.

Morris H, Gillingham MAF, Plavcová L, *et al.* 2018a. Vessel diameter is related to amount and spatial arrangement of axial parenchyma in woody angiosperms. Plant, Cell & Environment **41**, 245–260.

Morris H, Plavcová L, Gorai M, Klepsch MM, Kotowska M, Jochen Schenk H, Jansen S. 2018b. Vessel-associated cells in angiosperm xylem: highly specialized living cells at the symplast–apoplast boundary. American Journal of Botany **105**, 151–160.

Mrad A, Domec J-C, Huang C-W, Lens F, Katul G. 2018. A network model links wood anatomy to xylem tissue hydraulic behaviour and vulnerability to cavitation. Plant, Cell & Environment **41**, 2718–2730.

Nardini A, Salleo S, Trifilò P, Lo Gullo MA. 2003. Water relations and hydraulic characteristics of three woody species co-occurring in the same habitat. Annals of Forest Science **60**, 297–305.

Nardini A, Gascò A, Trifilò P, Lo Gullo MA, Salleo S. 2007. Ion-mediated enhancement of xylem hydraulic conductivity is not always suppressed by the presence of Ca^{2+} in the sap. Journal of Experimental Botany **58**, 2609–2615.

Nardini A, Battistuzzo M, Savi T. 2013. Shoot desiccation and hydraulic failure in temperate woody angiosperms during an extreme summer drought. New Phytologist **200**, 322–329.

Natale S, Tomasella M, Gargiulo S, Petruzzellis F, Tromba G, Boccato E, Casolo V, Nardini A. 2023. Stem photosynthesis contributes to non-structural carbohydrate pool and modulates xylem vulnerability to embolism in *Fraxinus ornus* L. Environmental and Experimental Botany **210**, 105315.

O'Brien MJ, Leuzinger S, Philipson CD, Tay J, Hector A. 2014. Drought survival of tropical tree seedlings enhanced by non-structural carbohydrate levels. Nature Climate Change **4**, 710–714.

Oparka KJ. 1994. Plasmolysis: new insights into an old process. New Phytologist **126**, 571–591.

Penttilä PA, Altgen M, Awais M, Österberg M, Rautkari L, Schweins R. 2020. Bundling of cellulose microfibrils in native and polyethylene glycol-containing wood cell walls revealed by small-angle neutron scattering. Scientific Reports **10**, 20844.

Peralta Ogorek LL, Song Z, Pellegrini E, Liu F, Tomasella M, Nardini A, Pedersen O. 2024. Root acclimations to soil flooding prime rice (*Oryza sativa* L.) for subsequent conditions of water deficit. Plant and Soil **494**, 529–546.

Petruzzellis F, Tordoni E, Di Bonaventura A, Tomasella M, Natale S, Bacaro G, Panepinto F, Nardini A. 2022. Turgor loss point and vulnerability to xylem embolism predict species-specific risk of drought-induced decline of urban trees. Plant Biology **24**, 1198–1207.

Pittermann J, Sperry JS, Wheeler JK, Hacke UG, Sikkema EH. 2006. Mechanical reinforcement of tracheids compromises the hydraulic efficiency of conifer xylem. Plant, Cell & Environment **29**, 1618–1628.

Plavcovà L, Hacke UG. 2011. Heterogeneous distribution of pectin epitopes and calcium in different pit types of four angiosperm species. New Phytologist **192**, 885–897.

Powell TL, Wheeler JK, de Oliveira AAR, da Costa ACL, Saleska SR, Meir P, Moorcroft PR. 2017. Differences in xylem and leaf hydraulic traits explain differences in drought tolerance among mature Amazon rainforest trees. Global Change Biology **23**, 4280–4293.

Salleo S, Hinckley TM, Kikuta SB, Lo Gullo MA, Weilgony P, Yoon TM, Richter H. 1992. A method for inducing xylem emboli *in situ*: experiments with a field-grown tree. Plant, Cell & Environment **15**, 491–497.

Sapes G, Demaree P, Lekberg Y, Sala A. 2021. Plant carbohydrate depletion impairs water relations and spreads via ectomycorrhizal networks. New Phytologist **229**, 3172–3183.

Savi T, Bertuzzi S, Branca S, Tretiach M, Nardini A. 2015. Drought-induced xylem cavitation and hydraulic deterioration: risk factors for urban trees under climate change? New Phytologist **205**, 1106–1116.

Schindelin J, Arganda-Carreras I, Frise E, *et al.* 2012. Fiji: an open-source platform for biological-image analysis. Nature Methods **9**, 676–682.

Schönbeck LC, Rasmussen C, Santiago LS. 2025. Leaf turgor loss does not coincide with cell plasmolysis in drought-tolerant Chaparral species. Plant, Cell & Environment **48**, 5019–5029.

Secchi F, Pagliarani C, Cavalletto S, *et al.* 2021. Chemical inhibition of xylem cellular activity impedes the removal of drought-induced embolisms in poplar stems – new insights from micro-CT analysis. New Phytologist **229**, 820–830.

Sevanto S, McDowell NG, Dickman LT, Pangle R, Pockman WT. 2014. How do trees die? A test of the hydraulic failure and carbon starvation hypotheses. Plant, Cell & Environment **37**, 153–161.

Silva LM, Pereira L, Kaack L, Guan X, Pfaff J, Trabi CL, Jansen S. 2024. The potential link between gas diffusion and embolism spread in angiosperm xylem: evidence from flow-centrifuge experiments and modelling. Plant, Cell & Environment **47**, 4977–4991.

Silva LM, Pfaff J, Pereira L, Miranda MT, Jansen S. 2025. Embolism propagation does not rely on pressure only: time-based shifts in xylem vulnerability curves of angiosperms determine the accuracy of the flow-centrifuge method. Tree Physiology. In press. doi:10.1093/treephys/tpae131.

Sinclair G, Galarneau ER, Hnizdor JF, McElrone AJ, Walker MA, Bartlett MK. 2024. Grape cultivars adapted to hotter, drier growing regions exhibit greater photosynthesis in hot conditions despite less drought-resistant leaves. Annals of Botany **134**, 205–218.

Sorek Y, Greenstein S, Netzer Y, Shtein I, Jansen S, Hochberg U. 2021. An increase in xylem embolism resistance of grapevine leaves during the growing season is coordinated with stomatal regulation, turgor loss point and intervessel pit membranes. New Phytologist **229**, 1955–1969.

Sorek Y, Greenstein S, Hochberg U. 2022. Seasonal adjustment of leaf embolism resistance and its importance for hydraulic safety in deciduous trees. Physiologia Plantarum **174**, e13785.

Tomasella M, Häberle K-H, Nardini A, Hesse B, Machlet A, Matyssek R. 2017. Post-drought hydraulic recovery is accompanied by non-structural carbohydrate depletion in the stem wood of Norway spruce saplings. Scientific Reports **7**, 14308.

Tomasella M, Casolo V, Aichner N, Petruzzellis F, Savi T, Trifilò P, Nardini A. 2019. Non-structural carbohydrate and hydraulic dynamics during drought and recovery in *Fraxinus ornus* and *Ostrya carpinifolia* saplings. Plant Physiology and Biochemistry **145**, 1–9.

Tomasella M, Petrussa E, Petruzzellis F, Nardini A, Casolo V. 2020. The possible role of non-structural carbohydrates in the regulation of tree hydraulics. International Journal of Molecular Sciences **21**, 144.

Tomasella M, Casolo V, Natale S, Petruzzellis F, Kofler W, Beikircher B, Mayr S, Nardini A. 2021. Shade-induced reduction of stem nonstructural carbohydrates increases xylem vulnerability to embolism and impedes hydraulic recovery in *Populus nigra*. New Phytologist **231**, 108–121.

Trifilò P, Nardini A, Gullo MAL, Barbera PM, Savi T, Raimondo F. 2015. Diurnal changes in embolism rate in nine dry forest trees: relationships with species-specific xylem vulnerability, hydraulic strategy and wood traits. Tree Physiology **35**, 694–705.

Trifilò P, Kiorapostolou N, Petruzzellis F, Vitti S, Petit G, Lo Gullo MA, Nardini A, Casolo V. 2019. Hydraulic recovery from xylem embolism in excised branches of twelve woody species: relationships with parenchyma cells and non-structural carbohydrates. Plant Physiology and Biochemistry **139**, 513–520.

Trueba S, Muñoz NG, Burlett R, *et al.* 2024. The rates of starch depletion and hydraulic failure both play a role in drought-induced seedling mortality. Annals of Forest Science **81**, 27.

Turner NC. 2018. Turgor maintenance by osmotic adjustment: 40 years of progress. Journal of Experimental Botany **69**, 3223–3233.

van Bel AJE. 1990. Xylem–phloem exchange via the rays: the undervalued route of transport. Journal of Experimental Botany **41**, 631–644.

Wang Y, Burlett R, Feng F, Tyree MT. 2014. Improved precision of hydraulic conductance measurements using a Cochard rotor in two different centrifuges. The Journal of Plant Hydraulics **1**, e007.

Wheeler JK, Sperry JS, Hacke UG, Hoang N. 2005. Inter-vessel pitting and cavitation in woody Rosaceae and other vesselled plants: a basis for a safety versus efficiency trade-off in xylem transport. Plant, Cell & Environment **28**, 800–812.

Yang D, Pan S, Ding Y, Tyree MT. 2017. Experimental evidence for negative turgor pressure in small leaf cells of *Robinia pseudoacacia* L versus large cells of *Metasequoia glyptostroboides* Hu et W.C.Cheng. 1. Evidence from pressure-volume curve analysis of dead tissue. Plant, Cell & Environment **40**, 351–363.

Zhang Y, Carmesin C, Kaack L, *et al.* 2020. High porosity with tiny pore constrictions and unbending pathways characterize the 3D structure of intervessel pit membranes in angiosperm xylem. Plant, Cell & Environment **43**, 116–130.

Zhu SD, Chen JY, Ye Q, He PC, Liu H, Li RH, Fu PL, Jiang GF, Cao KF. 2018. Leaf turgor loss point is correlated with drought tolerance and leaf carbon economics traits. Tree Physiology **38**, 658–663.

Zimmermann MH. 1983. Xylem structure and the ascent of sap. Berlin, Heidelberg: Springer-Verlag.